WWW.IJRPR.COM

International Journal of Research Publication and Reviews

Journal Homepage: www.ijrpr.com ISSN 2582-7421

Design and Real-Time Simulation of an EV Battery Charger

M. Vamsi Krishna[1], T. Pujitha[2], V. Dharma Sai[3]

[1-3]Department of Electrical and Electronics Engineering, GMR Institute of Technology (GMRIT), Rajam, India.
Email: vamsikrishnamittana@gmail.com

DOI : https://doi.org/10.55248/gengpi.07.1026.35012

A B S T R A C T

This article describes an electric-vehicle (EV) battery charger developed in MATLAB/Simulink and prepared for real-time execution on an OPAL-RT platform. The circuit consists of a single-phase source, a magnetically coupled input section, a universal-bridge rectifier, a half-bridge DC–DC stage built from two MOSFETs, an inductor–capacitor output filter, a lithium-ion battery block and PI-based current and voltage control paths. In the 10 s offline study the current reference is fixed at 6 A. The battery current climbs from zero to 6 A in roughly

0.3 s and then holds that value, while the terminal voltage moves from about 55.1 V to about 55.4 V. The charging power settles near 333 W, and the state of charge (SOC) advances from 40 % to about 40.11 %. All figures come from offline Simulink simulation and not from OPAL-RT measurements. The outcome confirms constant-current (CC) operation only; the constant-voltage (CV) stage, the CC-to-CV hand-over and reverse power flow were not exercised.

Keywords: EV battery charger, OPAL-RT, real-time simulation, synchronous buck converter, constant-current charging, PI control, state of charge (SOC), MATLAB/Simulink.

1. Introduction

As road transport moves away from combustion engines, the battery charger has become a key power-electronic component of an electric vehicle. It has to refill the pack quickly while staying inside the current and voltage limits set by the cell chemistry, keeping losses small, and remaining compatible with its supply [2], [3]. Lithium-ion packs are normally charged in two stages, CC followed by CV: a fixed current is forced until the terminal voltage reaches its ceiling, after which the voltage is held and the current is allowed to fall off [13].

A typical charger chains a coupling or isolation section, a rectifier and a DC–DC converter that matches the rectified DC-link level to the battery voltage. Bidirectional converters are especially useful here, since one power stage can both charge the battery and send energy back towards the DC link, which is the prerequisite for vehicle-to-grid (V2G) use [4]–[6]. Magnetic coupling at the input is likewise well studied: it supplies galvanic isolation and, when extended across an air gap, makes inductive wireless charging possible [7]–[9].

Simulation is normally the first checkpoint: the controller structure and its gains can be tuned on a model long before any hardware exists. For the battery, a dynamic representation is common, with terminal voltage determined by SOC and current [10], [11]; SOC also serves as the principal trigger for changing the charging mode [12], [14].

In this work a charger model is built in MATLAB/Simulink and prepared for real-time execution with OPAL-RT. The model contains an AC source, a mutual-inductance coupling, a universal-bridge rectifier, a two-MOSFET DC–DC converter, an L–C output filter, a battery and PI-based control paths. The waveforms reported below were obtained from offline Simulink simulation; hardware-captured OPAL-RT traces are not part of this manuscript. The contributions are:

- a description of the power stage and the control structure of the Simulink model;
- a 10 s constant-current simulation at a 6 A reference, used to examine how well the current loop tracks its command; and
- an interpretation of the resulting current, voltage, power and SOC waveforms.

Section 2 reviews earlier work, Section 3 explains the circuit and controllers, Section 4 presents and discusses the simulation results, and Section 5 closes the paper.

2. Literature Review

Ranjith Kumar et al. [1] provide a broad review of EV batteries, covering modelling, battery management, thermal management, SOC/SOH estimation and charge–discharge behaviour. A key message is that the charging strategy must be developed together with a faithful battery model and reliable SOC data.

Emadi et al. [2] gave an overview of the power electronics and motor drives found in electric, hybrid and plug-in hybrid vehicles, including the part played by DC–DC converters and chargers. Khaligh and Dusmez [3] compared conductive with inductive charging for plug-in vehicles and discussed the converter topologies suitable for each charger stage together with their trade-offs.

Bidirectional charging is mostly treated within V2G research. Yilmaz and Krein [4] examined how V2G affects distribution networks and which utility interfaces and chargers are required. Kisacikoglu et al. [5] evaluated bidirectional EV/PHEV chargers for reactive-power support, while Tan et al. [6] surveyed V2G technology and the optimisation methods used to bring EVs into smart grids.

Inductive power transfer (IPT) is a closely related field. Covic and Boys [7], [8] explained its operating principles and recent trends in transport, and Li and Mi [9] reviewed wireless charging of EVs. In such systems the coupling between two windings has the same role as the mutual-inductance section in the present model.

For the battery itself, Tremblay and Dessaint [10], [11] proposed a generic dynamic model for electric and hybrid vehicle simulation, in which the terminal voltage follows SOC and current. SOC estimation approaches were discussed by Hannan et al. [12] and Plett [14], and Notten et al. [13] investigated Li-ion fast charging that goes beyond the standard CC–CV profile.

Taken together, these studies show that the power stage, the controller and the battery model cannot be treated separately. The present work examines them in a single Simulink model that is also prepared for OPAL-RT execution, and uses the offline waveforms of current, voltage, power and SOC as a reference baseline.

3. System Description and Methodology

The charger is built in MATLAB/Simulink with the Specialized Power Systems blocks of Simscape Electrical and is intended for execution on OPAL-RT hardware. Figure 1 shows the complete circuit, including the power stage, the controllers and the measurement blocks.

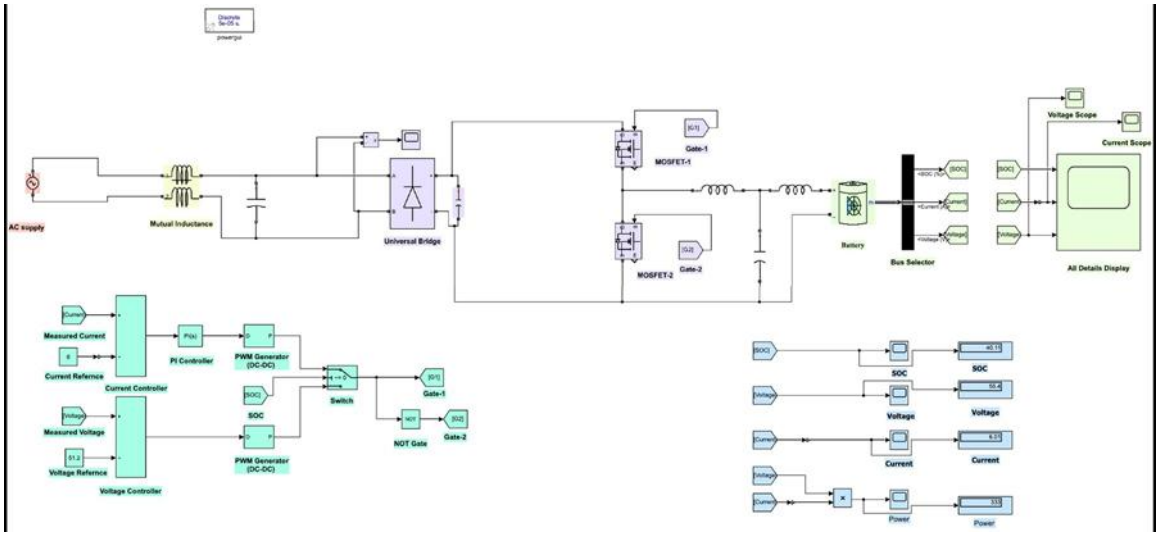


Figure 1. Complete Simulink schematic of the charger: power circuit, CC and CV controllers, SOC-driven switch and measurement displays.

3.1 System Architecture

Energy flows from the AC source through the mutual-inductance section and a shunt capacitor to the universal bridge, which rectifies it into the DC link. A half-bridge formed by MOSFET-1 and MOSFET-2 draws from this link, and its output is passed through two series inductors and a shunt capacitor (the L–C filter) on the way to the battery. A Bus Selector extracts SOC, current and voltage from the battery block and distributes them to the controllers, scopes and displays. Table 1 lists the role of each main block.

Table 1. Function of the principal blocks in the Simulink model.

Block	Function
AC supply	Single-phase source that feeds the charger.
Mutual inductance	Pair of coupled windings linking the source side to the rectifier side.
Filter capacitor	Shunt capacitor that reduces voltage ripple ahead of the rectifier.
Universal bridge	Rectifies the coupled AC voltage to produce the DC link.
MOSFET-1 / MOSFET-2	Upper and lower switches of the DC–DC half-bridge, fed by complementary pulses G1 and G2.
Series inductors and shunt capacitor	L–C output filter that limits current and voltage ripple at the battery.
Battery and Bus Selector	Stores the energy; the selector passes SOC, current and voltage to the controllers and displays.
Current controller and PI	Subtract the measured current from its reference and produce the duty-cycle command for CC mode.
Voltage controller	Compares battery voltage with its reference and produces the duty command for CV mode.
PWM generators (DC–DC)	Turn the duty commands into gate pulses for the switches.
Switch and NOT gate	SOC-based selection of CC or CV pulses for G1; inversion of G1 gives G2.

3.2 DC–DC Converter Topology

The two MOSFETs make up a synchronous half-bridge, with Gate-2 defined as the logical inverse of Gate-1 so that the switches conduct alternately. Since the DC link sits on the MOSFET side and the battery on the filter side, the stage works as a synchronous buck converter while charging, and its ideal mean output voltage is given by

$$V_o = D \cdot V_{dc} \qquad (1)$$

Here D denotes the duty ratio of Gate-1 and V_dc the DC-link voltage [15]. For a switching frequency f_s and a filter inductance L, the peak-to-peak inductor current ripple can be estimated as

$$\Delta I_L = (V_{dc} - V_o) \cdot D / (L \cdot f_s) \qquad (2)$$

and the L and C values are chosen so that the current and voltage ripple stay within the design limits [15]. A synchronous stage can in principle carry current in the reverse direction, but reverse power flow is not simulated here, so the topology by itself is not evidence of bidirectional operation.

3.3 Battery Model

The battery is modelled with the Simulink battery block, whose terminal voltage depends on SOC and battery current [10], [11]. SOC is obtained by integrating the current:

$$SOC(t) = SOC_0 + [100 / (3600\, Q_n)] \cdot \int i_b(\tau)\, d\tau \qquad (3)$$

In Equation (3) SOC is given in percent, SOC_0 is its starting value, Q_n is the rated battery capacity (Ah), t is in seconds and i_b is the charging current in amperes, taken as positive while charging. Dividing by 3600 converts ampere-hours to ampere-seconds. Because the expression simply counts charge, it presumes a fixed capacity and neglects coulombic efficiency and capacity-estimation error. SOC starts at 40 % here.

3.4 Control Strategy

Control is split into a current path and a voltage path. In the current path, the difference between the reference and the measured battery current is the error signal, which a PI controller converts into a duty ratio:

$$d(t) = K_p \cdot e(t) + K_i \int e(\tau)\, d\tau \qquad (4)$$

Here e(t) is the current error and d(t) the duty-ratio command sent to the PWM generator of the current loop. The voltage path works the same way but compares battery voltage with its own reference (51.2 V in this model) and feeds the second PWM generator. A switch driven by SOC decides which PWM output is used as Gate-1. During the 10 s run SOC changes by just 0.11 percentage points, which never reaches the switching level, so only the CC path acts. The study consequently shows current tracking in CC mode; CV regulation and a full CC–CV profile remain unverified. Before the converter is called a practical Li-ion charger, its switching rule and the safety of driving both gates in complement must be defined and tested.

A fixed 6 A reference is applied throughout the simulation. Starting from zero current, this lets the response speed and accuracy of the current loop be judged.

3.5 Simulation Setup

The offline Simulink model is simulated for 10 s with the ode23tb solver, and the powergui block runs in discrete mode with a 50 µs sample time. SOC, current and terminal voltage are logged through the Bus Selector, and the battery-side charging power is computed as the product of battery voltage and current. The charger was also run on OPAL-RT hardware, but the target configuration, real-time step size and captured outputs are not reported here, and no hardware figures are inferred from the offline settings. Table 2 lists the model settings stated in this work.

Table 2. Simulation settings used in the offline study.

Parameter	Value	Remarks
Supply frequency	50 Hz	Single-phase AC source
Battery type	Li-ion	Simulink battery block
Initial SOC	40 %	Start of the simulation
Current reference	6 A (constant)	CC mode
Voltage reference	51.2 V	Voltage-control branch
Powergui sample time	50 µs	Discrete mode
Solver / simulation time	ode23tb / 10 s	Offline study

4. Results and Discussions

This section presents the offline MATLAB/Simulink waveforms. Figure 2 groups the voltage, current, power and SOC traces, and Figures 3–6 show each quantity separately. The values quoted are approximate readings taken from the plots and must not be taken as OPAL-RT measurements. A hardware validation would compare current tracking, rise time, voltage response and SOC trend from OPAL-RT captures under the same reference.

4.1 Battery Current

Figure 3 shows the battery current. It starts at zero, rises almost linearly and reaches the 6 A reference after about 0.3 s, then stays at that value for the rest of the 10 s run. No overshoot, oscillation or steady-state error is visible, which indicates that the PI-based current loop follows its reference accurately. The final reading of the numeric display, 6.01 A, agrees with the reference.

4.2 Battery Terminal Voltage

Figure 4 gives the battery terminal voltage. It begins at about 55.1 V and climbs smoothly to about 55.4 V within roughly the first 1.5 s, after which it stays practically constant. This gradual, exponential-like rise follows the current ramp and reflects the internal dynamics of the battery model [10], [11].

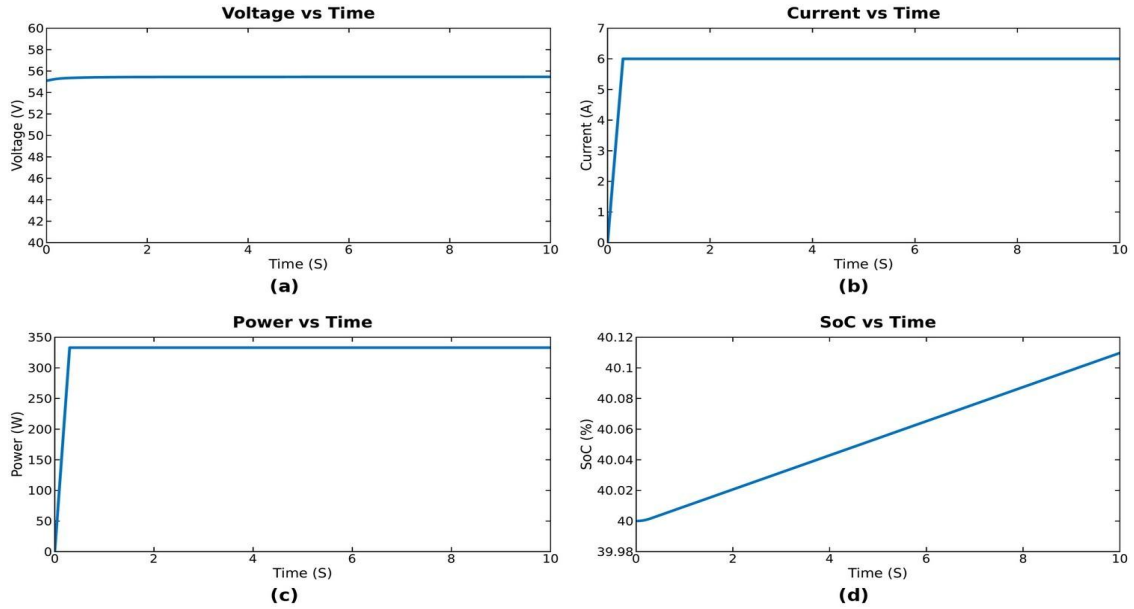


Figure 2. Combined view of the simulated battery quantities: (a) voltage, (b) current, (c) power and (d) SOC.

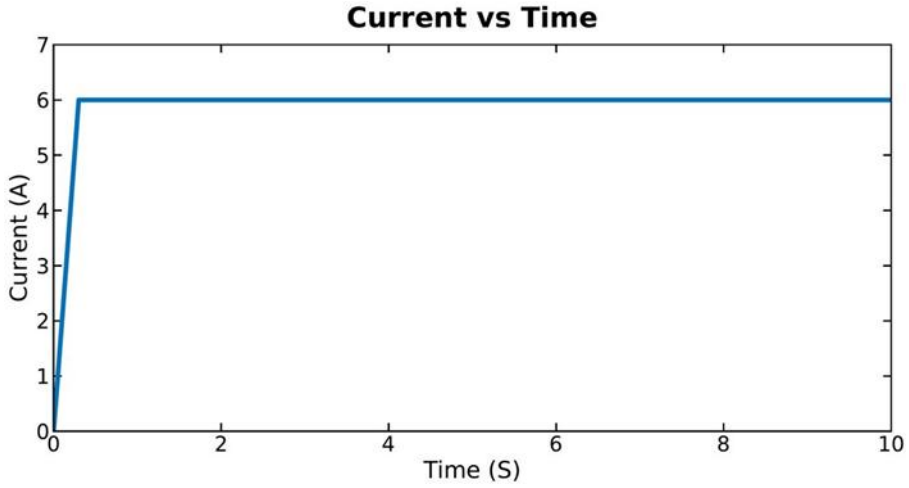


Figure 3. Battery charging current (A) for the constant 6 A reference.

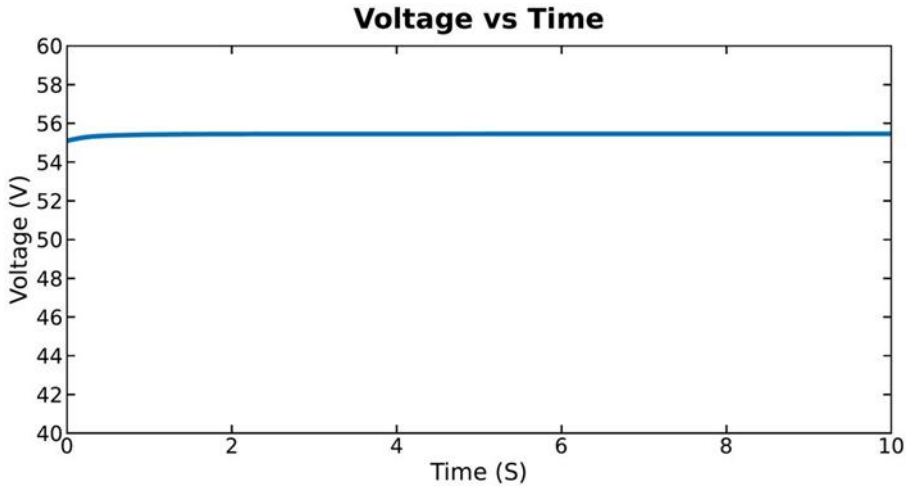


Figure 4. Battery terminal voltage (V).

The voltage increases by roughly 0.3 V while the current rises from 0 to 6 A, which is consistent with an effective series resistance of the order of 0.05 fi. The rise is therefore mostly the drop across the internal resistance of the battery, with the change in SOC contributing very little over such a short interval.

4.3 Charging Power

Charging power is the product of battery voltage and current and is plotted in Figure 5. It increases from zero together with the current and settles at about 333 W (6 A × 55.4 V), which matches the value shown on the power display. Because the voltage varies by well under 1 % after the initial rise, the power waveform has essentially the same shape as the current waveform.

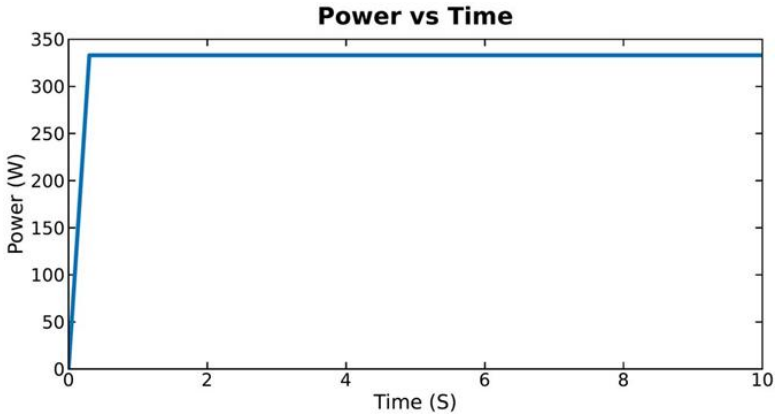


Figure 5. Power supplied to the battery during charging (W).

4.4 State of Charge

Figure 6 shows the SOC. It leaves 40 % with a short flat start and then climbs almost linearly to about 40.11 % at t = 10 s, a slope of about

0.011 %/s. A constant slope is what Equation (3) predicts for a constant current. Inserting this slope and i_b = 6 A into Equation (3) implies a rated capacity of about 15 Ah; this value is inferred from the plot and is not a stated model parameter.

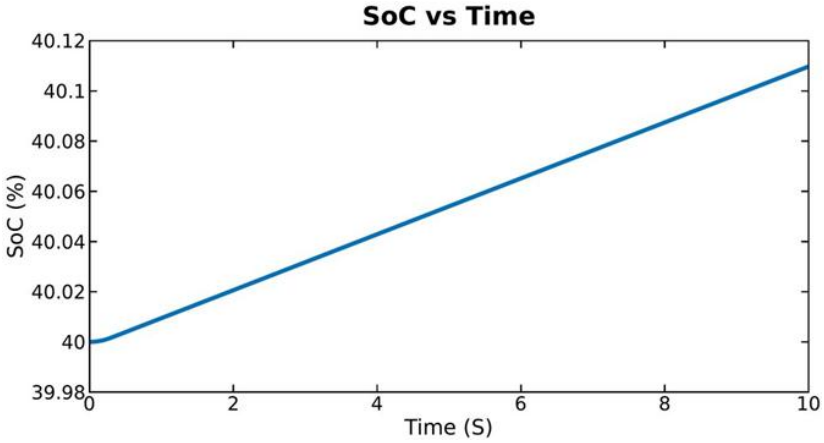


Figure 6. Battery state of charge (%).

4.5 Summary of Results

Table 3 collects the main quantities read from the simulation, separated into the start-up ramp (0–0.3 s) and the steady interval (0.3–10 s).

Table 3. Simulated charging results (approximate values read from the plots).

Quantity	Start-up (0–0.3 s)	Steady (0.3–10 s)	Remarks
Battery current	0 → 6 A	6 A	No visible overshoot
Battery voltage	≈ 55.1 → 55.4 V	≈ 55.4 V	Rise of ≈ 0.3 V
Charging power	0 → ≈ 333 W	≈ 333 W	P = V × I
SOC	≈ 40.00 %	≈ 40.11 % (t = 10 s)	Initial SOC = 40 %
SOC slope	≈ 0 (flat start)	≈ 0.011 %/s	Constant for constant current

In summary, the traces show a current loop that brings the battery current to 6 A promptly and keeps it there, with voltage, power and SOC changing smoothly. These findings are valid only for the plotted operating point and model settings. With SOC moving about 0.11 percentage points, the switching level is not reached, so CV mode stays untested. A longer run alone would not change this; a genuine CC-to-CV transition also needs a suitable battery model, voltage limit, switching logic and reference values.

5. Conclusion

An EV battery charger and its OPAL-RT workflow were presented using a MATLAB/Simulink model made up of a magnetically coupled input, a universal-bridge rectifier, a two-MOSFET DC–DC converter, an output filter, a battery block and PI-based controllers. With a 6 A reference in a 10 s offline run, the current reached 6 A after roughly 0.3 s and stayed there; the terminal voltage settled around 55.4 V, the power around 333 W, and SOC increased from 40 % to nearly 40.11 %. Since these are offline results, nothing is claimed about hardware performance until OPAL-RT recordings are added. The evidence covers CC-region current tracking only, not the CC-to-CV transition, reverse power flow or efficiency.

Prior to submission to a journal, the OPAL-RT target, solver, time step and run configuration should be recorded, and the captured hardware waveforms of current, voltage and SOC set against the offline baseline. Later work should show a CC-to-CV hand-over using a justified voltage limit and tested switching logic, examine reverse power flow if it is still claimed, and measure ripple and efficiency.

References

1. Ranjith Kumar, R., Bharatiraja, C., Udhayakumar, K., Devakirubakaran, S., Sekar, K. S., & Mihet-Popa, L. (2023). Advances in batteries, battery modeling, battery management system, battery thermal management, SOC, SOH, and charge/discharge characteristics in EV applications. IEEE Access, 11, 105761–105780.
2. Emadi, A., Lee, Y. J., & Rajashekara, K. (2008). Power electronics and motor drives in electric, hybrid electric, and plug-in hybrid electric vehicles. IEEE Transactions on Industrial Electronics, 55(6), 2237–2245.
3. Khaligh, A., & Dusmez, S. (2012). Comprehensive topological analysis of conductive and inductive charging solutions for plug-in electric vehicles. IEEE Transactions on Vehicular Technology, 61(8), 3475–3489.
4. Yilmaz, M., & Krein, P. T. (2013). Review of the impact of vehicle-to-grid technologies on distribution systems and utility interfaces. IEEE Transactions on Power Electronics, 28(12), 5673–5689.
5. Kisacikoglu, M. C., Ozpineci, B., & Tolbert, L. M. (2013). EV/PHEV bidirectional charger assessment for V2G reactive power operation. IEEE Transactions on Power Electronics, 28(12), 5717–5727.
6. Tan, K. M., Ramachandaramurthy, V. K., & Yong, J. Y. (2016). Integration of electric vehicles in smart grid: A review on vehicle to grid technologies and optimization techniques. Renewable and Sustainable Energy Reviews, 53, 720–732.
7. Covic, G. A., & Boys, J. T. (2013). Inductive power transfer. Proceedings of the IEEE, 101(6), 1276–1289.
8. Covic, G. A., & Boys, J. T. (2013). Modern trends in inductive power transfer for transportation applications. IEEE Journal of Emerging and Selected Topics in Power Electronics, 1(1), 28–41.
9. Li, S., & Mi, C. C. (2015). Wireless power transfer for electric vehicle applications. IEEE Journal of Emerging and Selected Topics in Power Electronics, 3(1), 4–17.
10. Tremblay, O., & Dessaint, L.-A. (2009). Experimental validation of a battery dynamic model for EV applications. World Electric Vehicle Journal, 3(2), 289–298.
11. Tremblay, O., Dessaint, L.-A., & Dekkiche, A.-I. (2007). A generic battery model for the dynamic simulation of hybrid electric vehicles. Proceedings of the IEEE Vehicle Power and Propulsion Conference (VPPC), 284–289.
12. Hannan, M. A., Lipu, M. S. H., Hussain, A., & Mohamed, A. (2017). A review of lithium-ion battery state of charge estimation and management system in electric vehicle applications: Challenges and recommendations. Renewable and Sustainable Energy Reviews, 78, 834–854.
13. Notten, P. H. L., Het Veld, J. H. G. O., & van Beek, J. R. G. (2005). Boostcharging Li-ion batteries: A challenging new charging concept. Journal of Power Sources, 145(1), 89–94.
14. Plett, G. L. (2004). Extended Kalman filtering for battery management systems of LiPB-based HEV battery packs: Part 1. Background. Journal of Power Sources, 134(2), 252–261.
15. Mohan, N., Undeland, T. M., & Robbins, W. P. (2003). Power Electronics: Converters, Applications, and Design (3rd ed.). John Wiley & Sons.